EFDA-JET-CP(06)05-21

C. Giroud, C. Angioni, G. Bonheure, I. Coffey, N. Dubuit, X. Garbet, R. Guirlet, P. Mantica, V. Naulin, M.E. Puiatti, M. Valisa, A.D. Whiteford, K-D. Zastrow, M.N.A. Beurskens, M. Brix, E. de la Luna, K. Lawson, L. Lauro-Taroni, A. Meigs, M. O'Mullane, T. Parisot, C. Perez Von Thun, O. Zimmermann and JET EFDA contributors

Progress in Understanding of Impurity Transport at JET

Progress in Understanding of Impurity Transport at JET

C. Giroud[1], C. Angioni[2], G. Bonheure[3], I. Coffey[4], N. Dubuit[5], X. Garbet[5], R. Guirlet[5], P. Mantica[6], V. Naulin[7], M.E. Puiatti[8], M. Valisa[8], A.D. Whiteford[9], K-D. Zastrow[1], M.N.A. Beurskens[1], M. Brix[1], E. de la Luna[10], K. Lawson[1], L. Lauro-Taroni[8], A. Meigs[1], M. O'Mullane[9], T. Parisot[5], C. Perez Von Thun[1], O. Zimmermann[11] and JET EFDA contributors*

[1]EURATOM-UKAEA Fusion Association, Culham Science Centre, Abingdon, OX14 3DB UK.
[2]Max-Planck-Institut für Plasmaphysik, EURATOM Association, D-85748 Garching, Germany.
[3]Association Euratom-Etat Belge, ERM-KMS, Brussels, Belgium.
[4]Department of Physics, Queens University, Belfast, BT7 1NN, U.K.
[5]CEA-Cadarache, Association Euratom-CEA, 13108 St Paul-lez-Durance France.
[6]Istituto di Fisica del Plasma, Associazione Euratom–ENEA–CNR, Milano, Italy.
[7]Association EURATOM-Risø National Laboratory, OPL-128, 4000 Roskilde Denmark.
[8]Consorzio RFX Associazione EURATOM-ENEA sulla Fusione, I-35127 Padova, Italy.
[9]Department of Physics, University of Strathclyde, Glasgow, G4 ONG, U.K.
[10]Asociación Euratom-CIEMAT, ES Avenida Complutense 22 E-28040 Madrid Spain.
[11]Forschungszentrum Jülich GmbH, IPP, Assoziation Euratom-FZJ, D-52425 Jülich Germany.
** See annex of M. L. Watkins et al, "Overview of JET Results",*
(Proc. 21st IAEA Fusion Energy Conference, Chengdu, China (2006)).

Preprint of Paper to be submitted for publication in Proceedings of the
21st IAEA Fusion Energy Conference,
(Chengdu, China, 16th October - 22nd October 2006)

ABSTRACT.
Experimental impurity transport coefficients in the core plasma are compared to predictions from turbulent transport theory, assuming a background turbulence induced by ion temperature gradient and trapped electron mode micro-instabilities. The effect of electron heating on impurity transport and the dependence on the charge of the impurity are studied.

1. INTRODUCTION

The design and operation of a future fusion power plant relies on the predictions of density and impurity profile in long pulse and in steady-state operation. Impurity densities set boundaries for the operational domain of an ITER plasma discharge. If the profile peaking of impurities becomes stronger than that of the main ions, i.e. if impurities accumulate, excessive fuel dilution occurs. An ITER plasma scenario also has to guarantee tolerable radiated power, a particular concern for highly charged impurities with a high associated cooling factor. Tungsten (W) concentration cannot exceed 10^{-4} in the core for stable plasma operation in ITER [1].

Within the set domain of viability, the design of an ITER scenario will require optimising opposing aspects of density peaking in the core plasma. It is advantageous to have a peaked density profile in a reactor as it provides an increase in fusion power and a higher bootstrap fraction, but the plasmas are prone to the peaking of highly charged impurities [1][2] [3]. An ITER plasma scenario will require optimising the density and impurity profiles to gain fusion power and pulse length, via bootstrap current, without detrimental fuel dilution or radiation losses [4] [5]. Therefore, it is necessary to understand the mechanisms driving impurity transport to have the means for controlling their profiles.

The radial impurity flux is expressed both with diffusive and convective contributions as follows:

$$\Gamma_{imp} = -D_{imp} \frac{\delta n_{imp}}{\delta r} + n_{imp} V_{imp}$$

where n_{imp}, D_{imp} and V_{imp} are respectively the impurity density, diffusion and convection coefficient (inwards if negative, and outwards if positive). In steady-state conditions and in plasma regions where the source can be neglected, the local logarithmic density gradient of an impurity ($1/L_{n_{imp}} = -d_{n_{imp}} /n_{imp} dr$) is directly related to the ratio of convection over the diffusion coefficient, V/D. Hence, the peaking of an impurity density is determined by the ratio $-V/D$, or equivalently the normalised peaking factor $-RV/D$ with R the plasma major radius. The understanding of this ratio as a function of the plasma radius is key to the control of impurity peaking.

Although a large number of experiments have been carried out to determine the transport coefficients for impurities, no clear description of impurity transport has yet emerged [6]. The lack of a theoretical framework to compare experimental findings may be at the origin. Indeed, neoclassical theory has failed to describe impurity transport across most of the plasma radius [6] [7], with the exception of two particular plasma regions. The impurity diffusion within a strong

internal transport barrier is observed to be close to its neoclassical value [3] and it is observed in ASDEX Upgrade that Tungsten (W) strongly accumulates in the plasma core in accordance with neoclassical theory [1].

Various observations made on anomalous impurity transport have encouraged the working hypothesis for ITER prediction, that anomalous diffusion is independent of the charge (Z) and mass (A) for low and medium Z impurity [6]. No recommendation has been made for high Z impurity. An additional observation that could be ascribed to anomalous transport is the fact that electron and ion cyclotron heating can affect impurity peaking [1] [2] [3] (and references in [7] and [8]). This effect has been observed on many devices over the last decade, but until recently remained without explanation.

Recent progress in the theory of turbulent transport provides a new framework in which experimental results can be compared. Over the past couple of years mechanisms on how microinstabilities can drive impurity transport have been identified.

In this paper, experimental transport coefficients are compared to predictions made by turbulent transport theory, assuming a background turbulence induced by Ion Temperature Gradient (ITG) and Trapped Electron Mode (TEM) micro-instabilities. Within this framework, we study both the effect of electron heating on impurity transport presented in section 2, and the dependence on the charge of the impurity presented in section 3.

2. PINCH REVERSAL OF NI IMPURITY WITH ELECTRON HEATING

Experiments have been performed at JET to influence the peaking of high Z impurities in ELMy H–mode plasma by changing from dominant ion heating to an increased electron heating [8]. Two Ion Cyclotron Resonance Frequency (ICRF) heating schemes were applied: ^{3}He Minority Heating (MH) delivering the largest amount of ICRF heating to the ions (with a concentration of ^{3}He ~8%), and ^{3}He Mode Conversion (MC) heating the electrons (with ^{3}He ~<20%). The main difference between the two pairs of H-mode discharges analysed is the radio-frequency scheme adopted, resulting in different power deposition in the electron channel shown in figure 1a. It is observed that in H-mode low collisionality discharges the transport behaviour of Nickel injected by laser blow-off is dramatically different. The transport coefficients have been determined by reproducing the spectroscopic measurements and are used to extrao□late to the steady-state profile of Ni shown in figure 1b, with a constant source. It is observed that the Ni profile is peaked in the MH scheme whereas it is slightly hollow or essentially flat in discharges with ICRF heating in MC. This different behaviour corresponds to different transport parameters.

Figures 1c shows differences in the diffusion profile between the two schemes. The diffusion coefficient in the MH shot is characterised by a central region with a diffusion of the same order as the neoclassical value, while in the MC shot the diffusion coefficient is well above the neoclassical value. It is also observed, in figure 1d that the velocity V changes direction from strongly inwards, in MH case, to slightly outwards, in MC case. This pinch reversal can only be attributed to anomalous transport as the neoclassical pinch velocity is directed inwards and does not change sign between MH and MC

discharges as shown in figure 1d. Moreover, the experimental values of the pinch velocity and diffusion are more than an order of magnitude higher than their neoclassical components. In these experiments, the transport of high charge impurity species Nickel is clearly anomalous.

The micro-instabilities present in the discharges have been identified with the linear version of the gyrokinetic code GS2. Although the ratio T_e/T_i of about 0.9 and logarithmic ion temperature gradient R/L_{Ti} are similar at mid-radius, the logarithmic density gradient R/L_n increases from 3.9 in the MH case to 5.2 in the MC case, similarly the logarithmic electron temperature gradient R/L_{Te} increases from about 4 to 6 respectively. The stability calculation shows that MH discharges are mainly ITG dominated, whereas the R/L_n driven TEM modes are the most unstable in the MC discharges. Ni transport resulting from such instabilities is calculated by a quasi-linear estimate with the linear version of GS2. It is found that calculated transport of Ni has an inward convection as observed experimentally. In the case of the TEM dominated MC discharges, the R/L_n driven TEM shows the possibility of a reduction of Ni peaking in comparison to the MH simulations but cannot imply a pinch reversal. However, it is possible to obtain a reversal of the calculated convection as observed experimentally in the following conditions. Figure 2 shows that if R/L_n is fixed and below its threshold and if the ITG instability is gradually switched off with a reduction of R/L_{Ti}, a change of sign of the peaking factor can be observed at high enough value of R/L_{Te}. The R/L_{Te} driven TEM instabilities can lead to a pinch reversal in qualitative agreement with experimental observations. This is explained by a mechanism of particle pinch connected with the parallel dynamics of the impurities [9] as discussed in more details in section 3.

The control and optimisation of impurity peaking relies in the understanding of the ratio of the diffusion to convection coefficients $-V/D$. Above, it was shown that electron heating is observed to decrease the ratio of $-V/D$ for Ni impurity and even to reverse its sign. A transition in the dominant instability driving Ni transport could be at the origin of this change. Below we show that the predicted ratio of $-V/D$ varies with the charge Z of the impurity, even in the case where only one micro-instability drives the transport.

3. Z DEPENDENCE OF IMPURITY TRANSPORT

The peaking factor predicted by theory of turbulent transport can have a complex dependence on the charge in varying plasma parameters as illustrated in figure 3. The normalised peaking factor, $-RV/D$, has been calculated with the linear version of the GS2 code for different Z in plasma conditions similar to the minority heating discharges presented in section 2. Figure 3 shows that the Z dependence of the peaking factor can have opposite sign for differing value of R/L_n: the peaking increases with an increasing impurity charge for the low value of R/L_n, whereas it increases with an increasing charge for high R/L_n. In particular the effect of an increase of R/L_n, for the plasma conditions studied here, is to increase the peaking of low Z impurity. This effect is in the same direction as neoclassical behaviour. Whereas the peaking of high Z impurity decreases as a result of the increased R/L_n in opposition to the neoclassical behaviour.

Recently, impurity transport has received an increased interest by theoreticians and progress has been made in the understanding of mechanisms involved in transport of impurity. With a simple fluid model and considering only electrostatic turbulence, three main mechanisms have been identified, each with its associated pinch contribution schematically represented in figure 4.

The first pinch, called curvature pinch [10][11][12], is caused by the compressibility effects of the $E \times B$ drift velocity in an inhomogeneous magnetic field. It is proportional to the gradient of the magnetic field and thus mostly inward for a monotonous increasing q profile and ballooning instabilities. The curvature pinch is independent of charge and mass. The second pinch velocity, the thermodiffusion pinch [9] [13][14],originates from the compression of the diamagnetic drift velocity and is proportional to the impurity temperature gradient. Its magnitude is inversely proportional to the charge of the species, and as a result the thermodiffusion pinch becomes negligible for high Z impurity. It has been calculated that the thermodiffusion mechanism is efficient for impurity with a charge below about 20 [9] [14]. The third pinch is connected with the parallel dynamics of the impurities [9]. The magnitude of this pinch is dependent on the ratio Z/A and thus in realistic cases independent of impurity species. (For the ionisation stage present at an electron temperature of 20keV correspond to a ratio Z/A varying from 1/2 for He to about 1/3 for W). This pinch was invoked in the calculation presented in section 2.

Although the curvature pinch is always inward, the thermodiffusion pinch and the pinch linked to the parallel velocity fluctuation can change sign depending on the direction of propagation of the instability, shown in figure 4. The thermodiffusion pinch is inward for transport driven by instability rotating in the electron diamagnetic direction, such as TEM, and outwards for transport driven by instability rotating in the ion diamagnetic direction such as ITG. In contrast, the pinch originating from the compression of parallel velocity has the opposite variation.

Therefore, the total pinch results for the sum of at least these three mechanisms and has a dependence on Z that is different for instability rotating in the ion or electron diamagnetic direction. The relative magnitude of these mechanisms can change depending on plasma conditions, such as q profile, or impurity temperature gradient. The turbulent transport is therefore complex even if only one instability is considered. In addition, a change of instability driving the transport complicates even further the dependence on Z of the transport coefficients. Figure 3 is a good illustration of this point. For low Z the thermodiffusion is active therefore the pinch from turbulent transport is directed outwards in the case of low value of R/L_n for which ITG are the most unstable mode. When R/L_n is increased, the dominant micro-instability changes to TEM for which the thermodiffusion is inwards, and as a result the peaking is increased. For large Z impurity, the thermodiffusion is negligible, and the reduction of peaking when changing from dominant ITG to TEM instability is most likely due to an increase of the diffusion coefficient. The complexity of the Z dependence require specific calculation of the diffusion and convection coefficients for comparison with the experiment.

3.1. EXPERIMENTAL DETERMINATION OF THE Z DEPENDENCE OF TRANSPORT COEFFICIENTS

The study of the Z dependence of impurity transport in various plasma conditions is performed by injecting three impurities Ne, Ar and Ni with respective Z of 10, 18 and 28 in the same discharge at a similar time. The density profile of Ne^{10+} and two ionisation stages of Ar, i.e. Ar^{16+}, Ar^{18+} are tracked simultaneously via the recently upgraded charge-exchange recombination spectroscopy diagnostic [15] with a time resolution of 10ms. The transport of Ni is inferred from the soft X-ray signals. The transport coefficients of these impurities are determined by re producing within UTC [16], the measured densities, soft x-ray signals and vacuum ultra-violet line intensities. Further details on the method used to determined the transport coefficients and an estimate of their uncertainty in this study is reported in [17].

The diffusion and convection coefficients have been determined experimentally for the Pulse No: 66134 with $R/L_{Ti} \sim< 5.8$, $R/L_{Te} \sim<6.3$, $R/L_n \sim< 0.3$ and $T_e/T_i \sim< 1.1$ and $\nu* \sim 0.10$. These transport coefficients are compared with the transport coefficients calculated with the linear version of GS2. The analysis of micro-instabilities reveals that the discharges is ITG dominated.

The measured Z dependence of the diffusion D, convection V coefficients and the peaking factor are shown in figure 5 for Pulse No: 66134 at different normalised radii, together with their neoclassical transport coefficients calculated with NCLASS. The measured diffusion coefficients of Ne, Ar and Ni are all an order of magnitude above their neoclassical level, both in the core and at mid-radius. The transport of these impurities is therefore anomalous. Figure 5a shows that the diffusion of Ne, Ar and Ni is reduced in the central region of the plasma inside $r/a \sim 0.2$. Inside this central region, the measured diffusion coefficient is dependent on Z, whereas outside this region is independent of the charge, as shown in figure 5a).

The measured convection coefficients are of the same magnitude as their neoclassical counterpart both in the core and at mid-radius as shown in figure 5b. It is interesting to note that the measured convections show a stronger dependence upon Z than the neoclassical velocity, the latter being only weakly dependent on the impurity charge.

The measured peaking factor, $\sim RV/D$, has a magnitude much smaller than its neoclassical value both in the core and at mid-radius as shown in figure 5c. For Ne, Ar and Ni, the measured peaking factor is positive (shown enlarged in figure 5c') without the neoclassical value, hence the impurities are peaked even if not as much as predicted by neoclassical theory. In contrast, the peaking factor of the intrinsic C is negative at mid-radius, but positive at the very centre r/a'~ 0.2. This results reflect a more general observation that at JET the C density profile is generally flat or hollow in ELMy H-mode discharges. The measured peaking factor increases weakly with Z in the region outside $r/a \sim 0.2$ whereas inside the measured peaking factor is showing a stronger dependence on the charge of the impurity.

3.2. COMPARISON WITH QUASILINEAR GYROKINETIC CALCULATION

The Z dependence of processes transporting impurity is specifically analysed for Pulse No: 66134 with the linear version of GS2 at mid-radius r/a ~ 0.55. The calculated diffusion, convection and peaking factor as shown in figure 6 and compared to their measured anomalous contributions, i.e. the neoclassical contribution has been subtracted from the measured diffusion and convection. The predicted diffusion and convection have been renormalised to the calculated deuterium diffusion coefficient to eliminate the uncertainty in the estimate of the saturation level of electrostatic potential.

The calculated peaking factor,*"RV/D*, is independent of such uncertainty and can be compared directly to the measured peaking factor. Figure 6a shows that the calculated diffusion coefficients decreases as the charge Z is increased from Deuterium (D) to C and becomes independent of the charge of the impurity. The diffusion of Ar and W are predicted to be equal from the theory of turbulent transport. Experimentally, it is observed that the anomalous Ne, Ar and Ni are similar within experimental errors, shown in figure 6a', in agreement with the predictions.

The calculated convection is shown to also decrease as Z is increased from D to about C and Ne after which it remains constant. The calculated convection is positive at low Z due to the outward contribution of the thermodiffusion. If the thermodiffusion is switched off by imposing R/L_{Tz} equal to 0 in the calculation, the convection is negative for all Z as shown in figure 6b. The measured anomalous convection, shown in figure 6b', is equal for Ne, Ar and Ni again in agreement with the calculations

As expected from a diffusion and convection coefficients becoming constant at high Z, the calculated peaking factor becomes also independent of the charge as shown in figure 6c. In contrast, the neoclassical peaking factor increases proportionally to Z as shown in figure 6c'. Experimentally, the measured anomalous peaking factor is closer in magnitude and behaviour to values calculated with the linear version of GS2 than predicted by neoclassical theory. The anomalous peaking factor is measured to be independent of the charge of Ne, Ar and Ni within experimental error in agreement with the calculated peaking factor. However, the measured anomalous peaking factor is of the same sign as the predictions but a factor 2 to 3 smaller. Impurities with charge below 3 are calculated to have a negative peaking as a result of the outward thermodiffusion to the total pinch shown in figure 6c. However, experimentally, C with a charge of 6 is observed to have a negative peaking at mid-radius, which could suggest that the thermodiffusion contribution is stronger than calculated by the linear version of GS2.

CONCLUSION

A pinch reversal for Ni impurity is observed when switching from minority heating to mode conversion heating. This pinch reversal could be explained qualitatively within the framework of ITG and TEM instabilities, by a transition in the dominant instability driving Ni transport and in particular to a pinch mechanism connected with the parallel dynamics of the impurities. The dependence of the transport coefficients on the charge of the impurity has also been studied for Ne, Ar and Ni. The transport of impurity is measured dominated by anomalous processes both in the

core region inside r/a ~ 0.2 and at mid-radius. However, a stronger dependence with the charge of the impurity is measured in the core plasma than at mid-radius. The measured peaking factor at mid-radius is closer in value to the predictions made by turbulent transport theory than neoclassical theory. The anomalous peaking factor is positive and independent of the charge for Ne, Ar and Ni as predicted by the linear gyrokinetic calculation, whereas C is negative in contrast with the prediction.

ACKNOWLEDGEMENTS

This work was partly supported by the United Kingdom Engineering and Physical Sciences Research Council and by the European Communities under the contract of Association between EURATOM and UKAEA. The views and opinions expressed herein do not necessarily reflect those of the European Commission. Part of this work is implemented under the International Energy Agency's cooperation agreement on Large Tokamak. The authors thank W.Dorland and M. Kotschenreuther for providing the gyrokinetic code GS2. One of the author thanks S. Knipe and L. Worth for the their help with the gas matrix, and Paula Belo for help using NCLASS.

REFERENCES

[1]. R. Neu *et al. Nucl. Fusion*, **45**: 209–218, 2005.
[2]. R Dux–*et al. Plasma Phys. Control. Fusion*, **45**:1815, 2003.
[3]. H. Takenaga *et al. Nucl. Fusion*, **43**:1235–1245, 2003.
[4]. C.D. Challis–*et al. Plasma Phys. Control. Fusion*, **46**:B23–B40, 2004.
[5]. H. Weisen–*et al.* IAEA Tech. Workshop on H-modes and transport barriers, 27.9.2005, subm. special PPCF conference issue.
[6]. ITER Physics Expert Groups *et al. Nucl. Fusion*, **39**(12):2225, 1999.
[7]. R. Guirlet *et al. subm. special PPCF conference issue EPS*, 2006.
[8]. M.E. Puiatti *et al. Phys. Plasmas*, **13**:042501, 2006.
[9]. C. Angioni *et al. PRL*, **96**:095003, 2006.
[10]. V.V. Yankov *et al. JETP LETT.*, **60**:171, 1994.
[11]. M.B. Isichenko *et al. Phys. Rev. Lett.*, **74**:4436, 1996.
[12]. V. Naulin *et al. Phys. Rev. E.*, **71**:015402(R), 2005.
[13]. X. Garbet *et al. Phys. Plasmas*, **12**:082511, 2005.
[14]. N. Dubuit *et al. Submitted to Phys. Plasmas*, 2006.
[15]. C. Negus *et al. to be published in Rev. Sci. Inst.*, 2006.
[16]. A.D. Whiteford. PhD thesis, University of Strathclyde, 2004.
[17]. C. Giroud *et al. Submitted to Nucl. Fusion*, 2006.

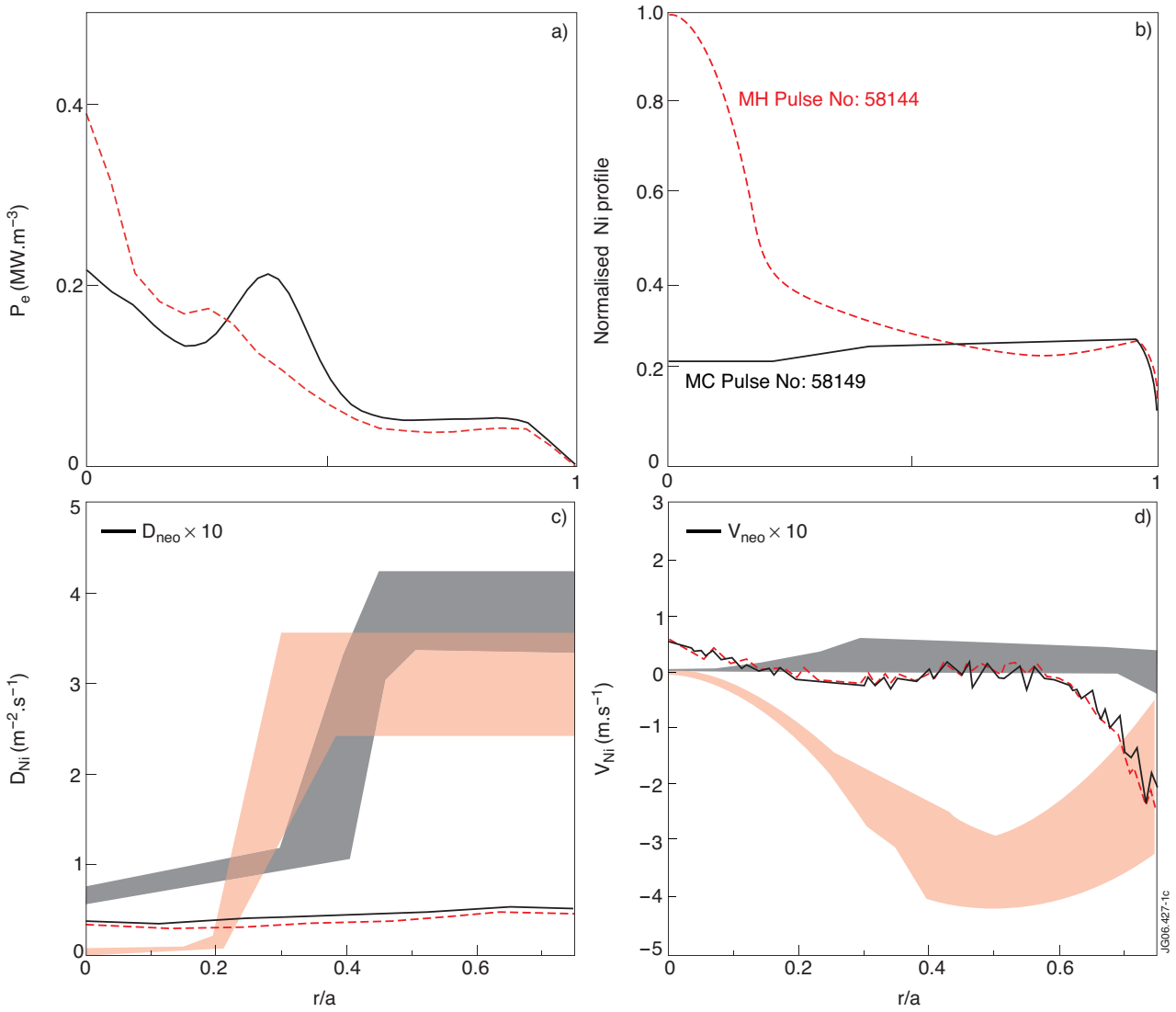

Figure 1: Comparison of Ni transport in ELMy H-modes with ICRH ^{3}He Mode Convection (MC) heating and Minority Heating (MH). the MC Pulse No: 58149 is shown in blue and the MH Pulse No: 58144 in red and neoclassical values in dashed lines: shown are the profiles for a) the electron power deposition profiles. b) steady-state of Ni density as obtained from an extrapolation of determined transport coefficients. c) the measured diffusion coefficient, d)the measured convection coefficient with their neoclassical values. The coloured areas represent the error estimate of the transport coefficients.

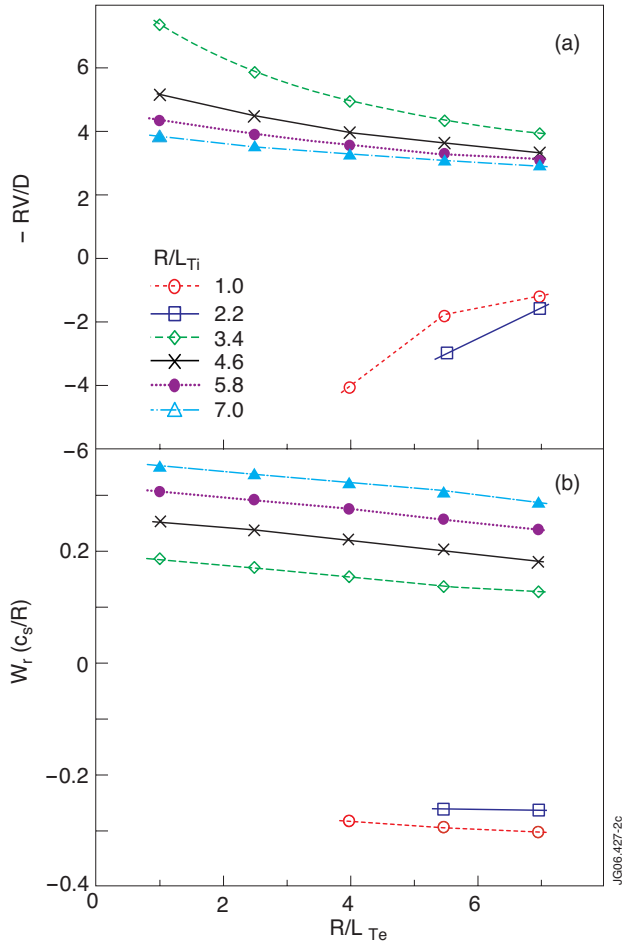

Figure 2: GS2 calculation of Ni peaking factor –RV/D (a) and real frequency of the most unstable mode (b) as a function of the logarithmic electron temperature gradient R/L_{Te} for six values of the logarithmic ion temperature gradient R/L_{Ti}, with fixed R/L_n=2.

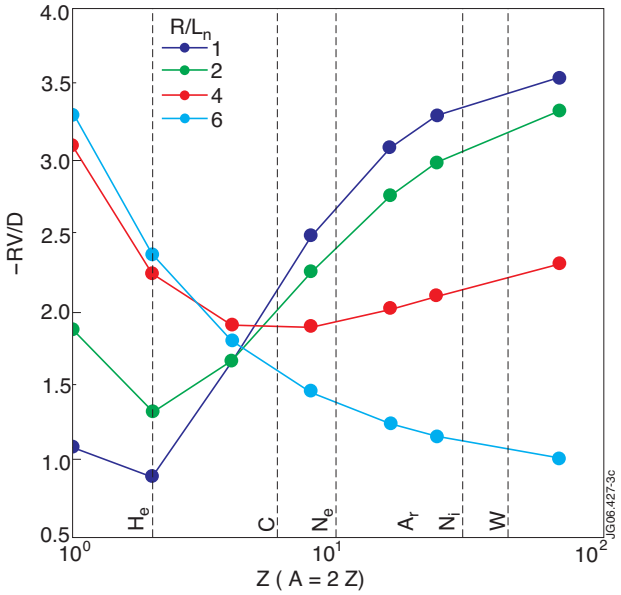

Figure 3: GS2 calculation of peaking factor (–RV/D) as a function of the charge Z of an impurity with a mass A equal to twice its charge for four values of the logarithmic density gradient R/L_n, with fixed R/L_{Te} and R/L_{Ti}.

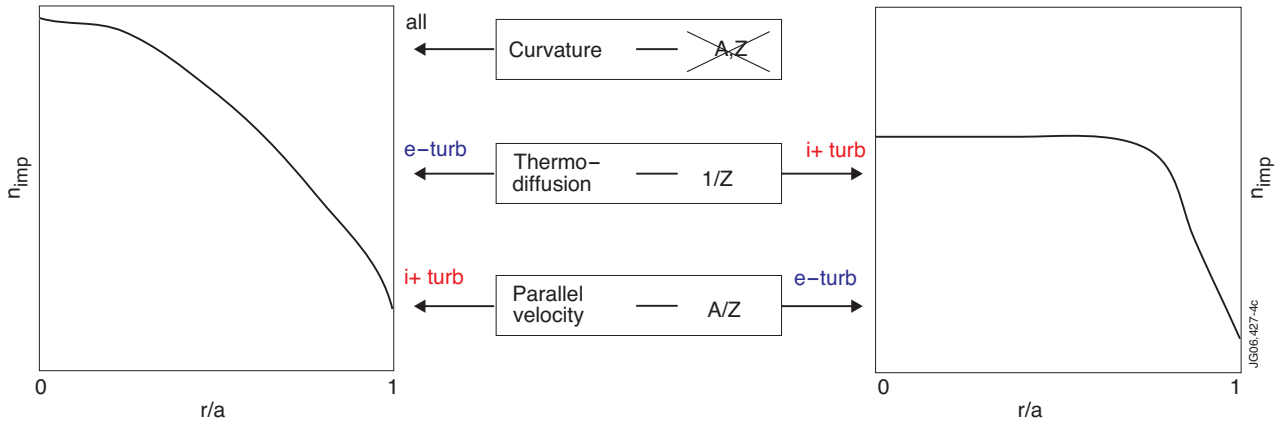

Figure 4: Schematic of current understanding of three additive terms forming the turbulent pinch indicating the main dependence of each term, how each term can influence impurity peaking and if it depends on the direction of propagation of the dominant instability rotating in the ion or electron diamagnetic direction.

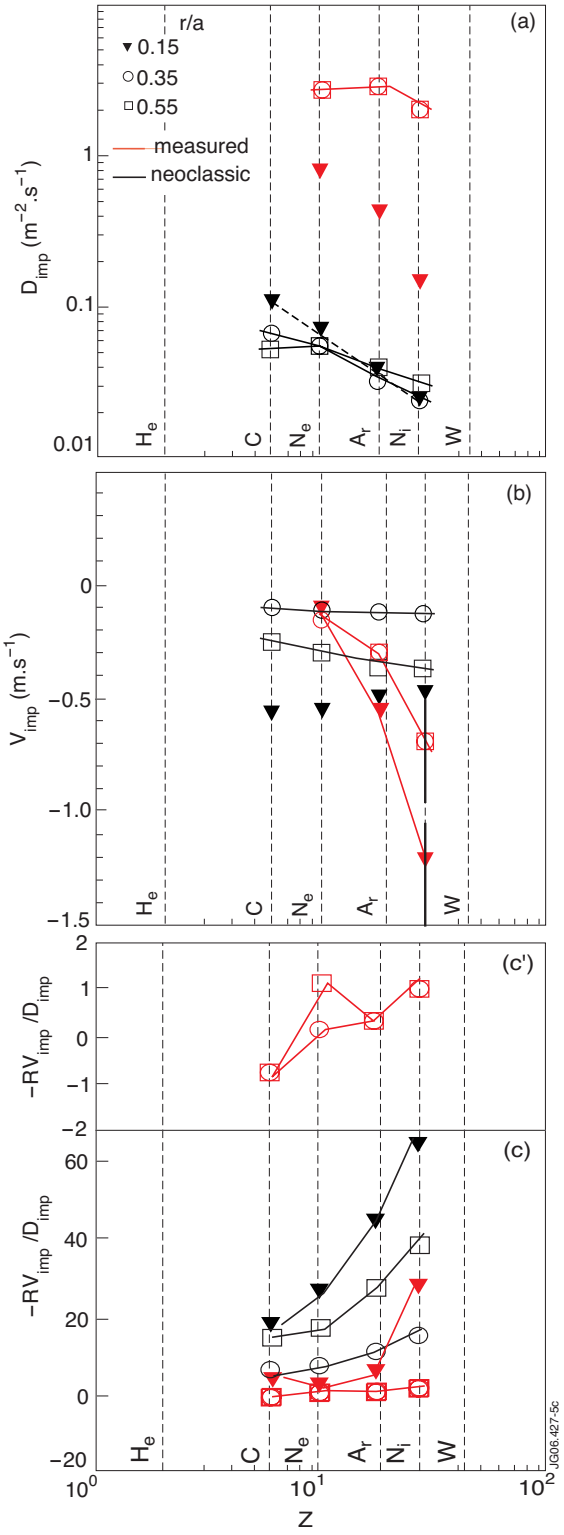

Figure 5: Comparison of the measured Z dependence of transport coefficients for Pulse No: 66134 at different normalised radii. The measurements are shown in red symbols with a black error bar and the neoclassical value in black symbols. Shown in a) are the diffusion coefficient, in b) the convection coefficient, in c) and c') the peaking factor.

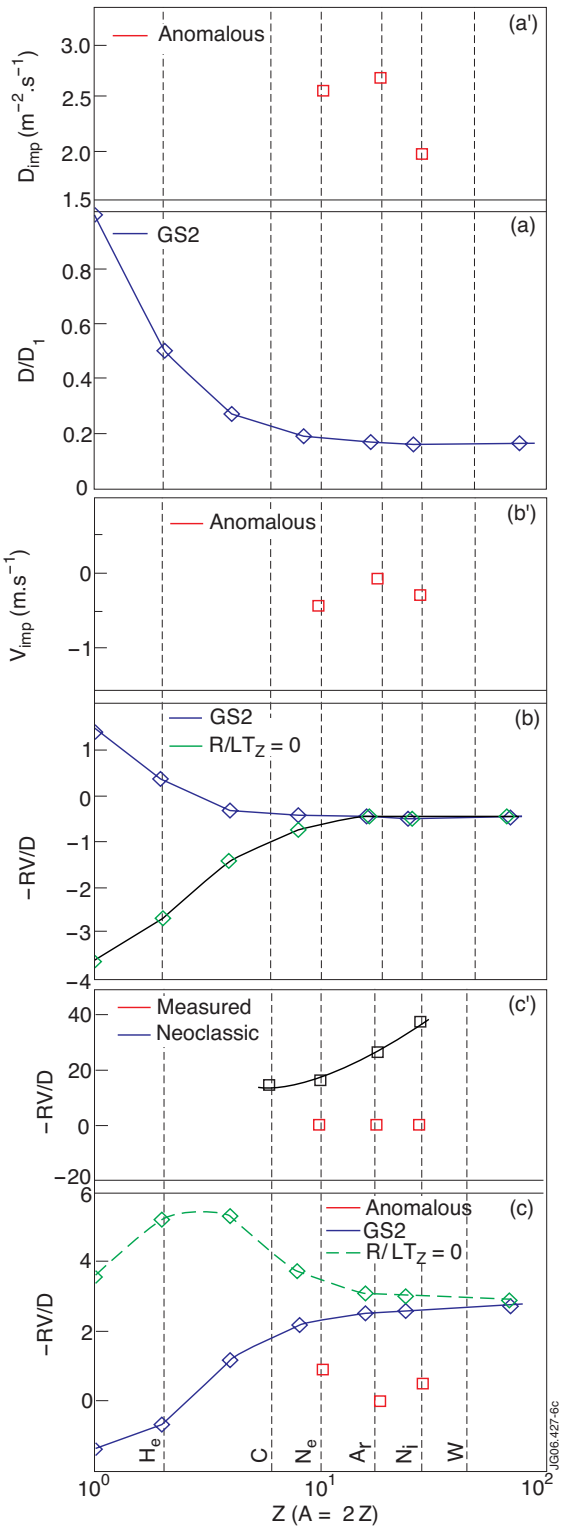

Figure 6: Comparison of the measured anomalous transport coefficients for Pulse No: 66134 with the GS2 calculation at mid-radius r/a ~0.55. The measurements are shown in red, the GS2 result in blue with thermodiffusion and in green without. Shown are in a) the diffusion coefficient, in b) the convection coefficient, in c) the peaking factor. Shown in c') is the comparison with neoclassical predictions.